J Electr Eng Technol.2018; 13(4): 1566-1577
http://doi.org/10.5370/JEET.2018.13.4.1566

ISSN(Print) 1975-0102
ISSN(Online) 2093-7423

Modelling and Stability Analysis of AC-DC Power Systems Feeding a Speed Controlled DC Motor

Jakkrit Pakdeeto*, Kongpan Areerak† and Kongpol Areerak*

Abstract – This paper presents a stability analysis of AC-DC power system feeding a speed controlled DC motor in which this load behaves as a constant power load (CPL). A CPL can significantly degrade power system stability margin. Hence, the stability analysis is very important. The DQ and generalized state-space averaging methods are used to derive the mathematical model suitable for stability issues. The paper analyzes the stability of power systems for both speed control natural frequency and DC-link parameter variations and takes into account controlled speed motor dynamics. However, accurate DC-link filter and DC motor parameters are very important for the stability study of practical systems. According to the measurement errors and a large variation in a DC-link capacitor value, the system identification is needed to provide the accurate parameters. Therefore, the paper also presents the identification of system parameters using the adaptive Tabu search technique. The stability margins can be then predicted via the eigenvalue theorem with the resulting dynamic model. The intensive time-domain simulations and experimental results are used to support the theoretical results.

Keywords: Stability, Model, DC motors, Constant power load, DQ method, Generalized state-space averaging method, Identification, Adaptive Tabu search.

1. Introduction

It is well-known that DC motors are widely used in the most control systems such as electrical system in vehicles, trains and homes [1]. Unfortunately, the speed controlled DC motor behaves as a constant power load (CPL). This CPLs can reduce the damping of the system and significantly degrade the system stability [2-4]. Without stability study, the system may become unstable under the rated operation. Therefore, the stability analysis of power systems with the DC motor speed control is very important. The mathematical model of the power system with CPL is required for stability studies. Normally, the model of power converter is time-varying because of the switching behavior in which it is very complicated for the stability analysis. Several approaches are used to eliminate the switching action to achieve the time-invariant model. As a result, the classical control theory such as the eigenvalue theorem can be applied to predict the unstable operation. In this paper, the AC and DC distribution systems connected together via a six-pulse diode rectifier are used to supply power to the speed controlled DC motor. For stability studies, the rectifier unit can normally be modeled as a constant DC voltage source by ignoring the dynamic of rectifier including the AC transmission parameters. However, this approach is not precise and cannot confirm the correct unstable point [5, 6]. As for the controlled DC motor, it behaves as the CPL. This load can simply be considered as a voltage-dependent current source under the assumption that the fast controller actions are obtained. Therefore, the ideal CPLs by ignoring their dynamics were used for the stability analysis in many research works [7, 8].

To achieve more precise stability results, this paper will present how to derive the dynamic model of the proposed power system via the DQ [9-11] and the generalized state-space averaging (GSSA) [12-14] methods. According to the proposed technique, both six-pulse rectifier with AC transmission lines and controlled speed motor dynamics can be taken into account in the resulting model in which it has not been reported in the previous publications. Furthermore, according to considering the dynamic of CPL, the results will show later that the speed control natural frequency can significantly affect the stability margin. In the area of stability analysis due to CPLs, most research works [15-17] focus on only how to determine the mathematical model and how to analyze the stability of the system. Then, the intensive time-domain simulations via well-known software packages are used to verify the unstable point predicted from the theory. However, for the practical systems, accurate mathematical models without accurate system parameters are not sufficient to predict the unstable point. The system parameters of practical systems are required. From the literatures the artificial intelligent (AI) techniques such as genetic

† Corresponding Author: Power electronics, Energy, Machines and Control Research Group, School of Electrical Engineering, Suranaree University of Technology, Thailand. (kongpan@sut.ac.th)
* Power electronics, Energy, Machines and Control Research Group, School of Electrical Engineering, Suranaree University of Technology, Thailand.
Received: July 4, 2017; Accepted: February 26, 2018

algorithm (GA), particle swarm optimization (PSO) and adaptive Tabu search algorithm (ATS) are suitable to identify the parameters of the system. Moreover, the ATS algorithm has the mathematical proof to ensure that the solution from the ATS method can escape the local solution [18]. Hence, this paper presents how to apply the ATS algorithm [19, 20] to identify the system parameters. Consequently, the resulting dynamic model with the identified system parameters is conveniently used with the eigenvalue theorem to predict the instability. The procedures described in the paper may be considered as a powerful and flexible tool to analyze the stability of practical power systems having CPLs.

The paper is structured as follows. In Section 2, the power system definition and the dynamic model of the considered power system by using the DQ and GSSA modeling methods is explained. In Section 3, the system parameter identification of the testing rig using the ATS algorithm is described. The model validation using the identified parameters is also given in Section 3. In Section 4, the stability analysis via the eigenvalue theorem is addressed with the simulation and experimental results. The effects of DC-link parameters and natural frequency of speed control on the stability margin are also illustrated in Section 4. Finally, Section 5 concludes and discusses the advantages of the proposed procedure to predict the unstable point of practical power systems.

2. Dynamic Model of Considered System

2.1 Power system definition

The considered power system is depicted in Fig. 1. It consists of a balanced three-phase voltage source, transmission line, three-phase diode rectifier, and DC-link filters feeding a speed controlled DC motor. The buck converter with a PI controller is used to regulate the DC motor speed via the armature circuit, while the field voltage V_f is fixed at the rated voltage. The speed controlled DC motor behaves as CPL in which it can significantly degrade the system stability as mentioned before. For deriving the dynamic model, it is assumed that the diode rectifier and the buck converter are operated under a continuous conduction mode (CCM) and the higher harmonics of the fundamental are neglected.

2.2 Mathematical model derivation

In this paper, the DQ method is firstly selected to derive the dynamic model of a three-phase diode rectifier feeding uncontrolled buck converters (open-loop operation) in which such rectifier can be treated as a transformer [9]. As a result, the equivalent circuit of the power system of Fig. 1 (without controllers of buck converters) can be represented in the DQ frame as depicted in Fig. 2. Note

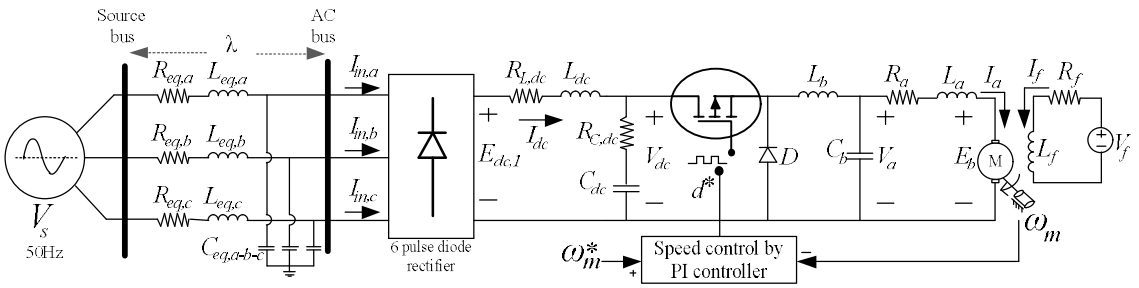

Fig. 1. The considered power system

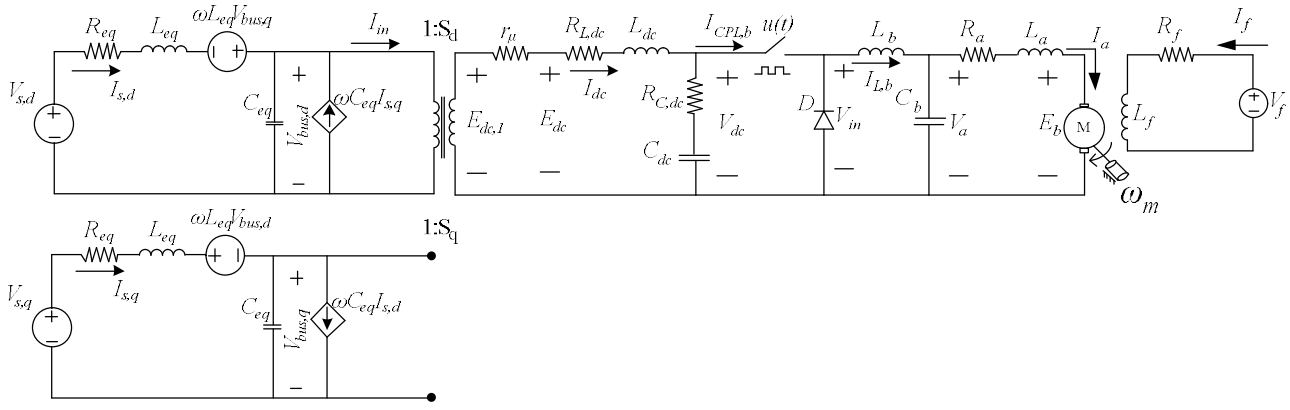

Fig. 2. The equivalent circuit on DQ frame under open-loop operation of buck converter

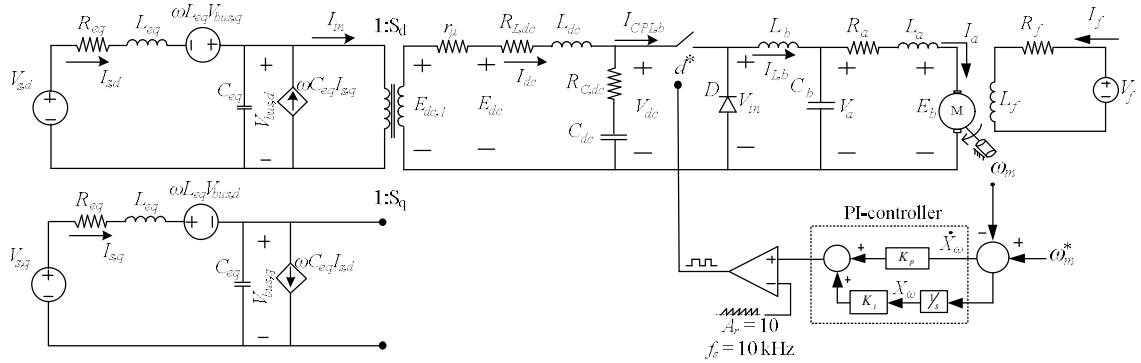

Fig. 3. The equivalent circuit of considered power system on DQ frame including a speed control

that the equivalent circuit in Fig. 2 is simplified by fixing the rotating frame on the phase of diode rectifier switching function. The more details how to derive the three-phase diode rectifier as the transformer using the DQ method can be found in [21]. As can be seen from Fig. 2, the DQ method can eliminate the switching action of the diode rectifier. Consequently, the diode rectifier can be modeled as the transformer with the constant ratio in which it can provide the time-invariant model. The GSSA method is then used to eliminate the switching action of the uncontrolled buck converter in the armature circuit of DC motor. The dynamic model of the system in Fig. 2 using GSSA method can be obtained with parameter d, duty cycle of buck converter. The more details how to derive the buck converter using the GSSA method can be found in [13].

According to applying the GSSA method, the model is the time-invariant in which the switching behaviors of the diode rectifier and buck converter are already eliminated. For deriving the mathematical model of the power system including dynamic of DC motor speed control, the schematic of the PI controller is considered. The equivalent circuit of Fig. 2 becomes to the new circuit as shown in Fig. 3. It can be seen that the PI controller represented by K_p and K_i is occurred. From Fig. 3, d^* can be derived and given in (1).

$$d^* = \frac{1}{A_r}\left(K_p\omega_m^* - K_p\omega_m + K_i X_\omega\right) \tag{1}$$

In Fig. 3, when PI controller is considered, the X_ω of speed control is set as the state variable of the model. Moreover, when the buck converter is regulated, the d in the model of Fig. 2 becomes d^* as given in (1). Therefore, applying d^* from (1) into d and adding the state variable of PI controller, the dynamic model of the system in Fig. 3 can be expressed in (2)

It can be seen in (2) that when we consider the speed controlled DC motor, the PI controller parameters are included in the dynamic model. In addition, the state variable X_ω is also included. Eq. (2) is the nonlinear differential equations. To analyze the stability by using the eigenvalue theorem, (2) is therefore linearized by the first order terms of Taylor series expansion so as to achieve a set of linear differential equations around an equilibrium point. After applying the linearization technique, (2) is then of the form in (3)

$$\begin{cases}
\dot{I}_{s,d} = -\dfrac{R_{eq}}{L_{eq}}I_{s,d} + \omega I_{s,q} - \dfrac{V_{bus,d}}{L_{eq}} + \sqrt{\dfrac{3}{2}}\dfrac{V_m\cos\lambda}{L_{eq}} \\
\dot{I}_{s,q} = -\omega I_{s,d} - \dfrac{R_{eq}}{L_{eq}}I_{s,q} - \dfrac{V_{bus,q}}{L_{eq}} + \sqrt{\dfrac{3}{2}}\dfrac{V_m\sin\lambda}{L_{eq}} \\
\dot{V}_{bus,d} = \dfrac{I_{s,d}}{C_{eq}} + \omega V_{bus,q} - \sqrt{\dfrac{3}{2}}\cdot\dfrac{2\sqrt{3}}{\pi\cdot C_{eq}}I_{dc} \\
\dot{V}_{bus,q} = \dfrac{I_{s,q}}{C_{eq}} - \omega V_{bus,d} \\
\dot{I}_{dc} = \sqrt{\dfrac{3}{2}}\cdot\dfrac{2\sqrt{3}}{\pi\cdot L_{dc}}V_{bus,d} - \dfrac{(r_\mu + R_{L,dc} + R_{C,dc})}{L_{dc}}I_{dc} \\
\quad - \dfrac{V_{dc}}{L_{dc}} + \dfrac{K_p\omega_m^*\cdot R_{C,dc}}{A_r\cdot L_{dc}}I_{L,b} - \dfrac{K_p\omega_m\cdot R_{C,dc}}{A_r\cdot L_{dc}}I_{L,b} \\
\quad + \dfrac{K_i X_\omega\cdot R_{C,dc}}{A_r\cdot L_{dc}}I_{L,b} \\
\dot{V}_{dc} = \dfrac{I_{dc}}{C_{dc}} - \dfrac{K_p\omega_m^*\cdot R_{C,dc}}{A_r\cdot C_{dc}}I_{L,b} + \dfrac{K_p\omega_m\cdot R_{C,dc}}{A_r\cdot C_{dc}}I_{L,b} \\
\quad - \dfrac{K_i X_\omega\cdot R_{C,dc}}{A_r\cdot C_{dc}}I_{L,b} \\
\dot{I}_{L,b} = -\dfrac{K_p\omega_m^*\cdot R_{C,dc}}{A_r\cdot L_b}V_{dc} + \dfrac{K_p\omega_m\cdot R_{C,dc}}{A_r\cdot L_b}V_{dc} \\
\quad - \dfrac{K_i X_\omega\cdot R_{C,dc}}{A_r\cdot L_b}V_{dc} - \dfrac{V_a}{L_b} \\
\dot{V}_a = \dfrac{I_{L,b}}{C_b} - \dfrac{I_a}{C_b} \\
\dot{I}_a = \dfrac{V_a}{L_a} - \dfrac{R_a}{L_a}I_a - \dfrac{K_v I_f}{L_a}\omega_m \\
\dot{I}_f = -\dfrac{R_f}{L_f}I_f + \dfrac{V_f}{L_f} \\
\dot{\omega}_m = \dfrac{K_t I_f}{J}I_a - \dfrac{B}{J}\omega_m - \dfrac{T_L}{J} \\
\dot{X}_\omega = \omega_m^* - \omega_m
\end{cases} \tag{2}$$

$$\begin{cases} \delta \dot{\mathbf{x}} = \mathbf{A}(\mathbf{x_o},\mathbf{u_o})\delta\mathbf{x} + \mathbf{B}(\mathbf{x_o},\mathbf{u_o})\delta\mathbf{u} \\ \delta\mathbf{y} = \mathbf{C}(\mathbf{x_o},\mathbf{u_o})\delta\mathbf{x} + \mathbf{D}(\mathbf{x_o},\mathbf{u_o})\delta\mathbf{u} \end{cases} \quad (3)$$

The constant matrixes $\mathbf{A}(\mathbf{x_o},\mathbf{u_o})$, $\mathbf{B}(\mathbf{x_o},\mathbf{u_o})$, $\mathbf{C}(\mathbf{x_o},\mathbf{u_o})$, and $\mathbf{D}(\mathbf{x_o},\mathbf{u_o})$ depend on the chosen equilibrium point. The details of these matrixes can be found in the Appendix. According to linearized model in (3), the model needs to define $I_{L,b0}$, $V_{dc,0}$, $\omega^*_{m,o}$, $\omega_{m,o}$ $X_{\omega,0}$. In the paper, the power flow equation can be first applied to determine the steady state values at the AC side [21], here are $V_{bus,o}$ and λ_o. Other steady-state values can be then calculated by (4)

$$\begin{cases} V_{dc,0} = \dfrac{3\sqrt{3}(\sqrt{2}V_{bus,0})}{\pi} \\ I_{L,b0} = \dfrac{T_L}{K_t I_f} \\ \omega_{m,0} = \omega^*_{m,0} \\ X_{\omega,0} = \dfrac{\dfrac{R_a T_L}{K_t I_f} + K_v I_f \omega^*_{m,0}}{V_{dc,0}\cdot K_i} \end{cases} \quad (4)$$

3. System Parameter Identification

As mentioned in Section 1, the precise dynamic model is not sufficient for the stability analysis of practical systems. The accurate system parameters are also required. In this paper, the experimental results will be used to validate the unstable point predicted from the theory. Therefore, the experimental test rig related to the considered system of Fig. 1 is set up as shown in Fig. 4. The PI controller of the rig was implemented using microcontroller AVR, ATmaga1280, ET-EASY MEGA1280. The diode rectifier and the buck converter have been constructed using 10 A, 500 V and 45 A, 650 V converter modules, respectively. Low cost electrolytic capacitors were used to implement the DC bus voltage. In this section, parameters of the test rig determined by a measurement and identification techniques using the ATS algorithm are presented. From (3) where

$$\delta\mathbf{x} = [\delta I_{s,d}\ \delta I_{s,q}\ \delta V_{bus,d}\ \delta V_{bus,q}\ \delta I_{dc}\ \delta V_{dc}\ \delta I_{L,b}\ \delta V_a\ \delta I_a\ \delta I_f\ \delta\omega_m\ \delta X_\omega]^T$$
$$\delta\mathbf{u} = [\delta V_m\ \delta V_f\ \delta T_L\ \delta\omega^*_m]^T$$
$$\delta\mathbf{y} = [\delta V_{dc}\ \delta I_a\ \delta\omega_m]^T$$

Before testing, the parameters of the rig need to be determined, especially R_{eq}, L_{eq}, $R_{L,dc}$, L_{dc}, $R_{c,dc}$, C_{dc} and DC motor parameters. The AC power system is assumed to be a balanced system. Therefore, the three-phase line parameters are identical and set equal to R_{eq}, L_{eq}, and C_{eq}. It can be seen in Fig. 1, the system identification process can be divided into two parts by setting the border after DC-link filters. The first part is called the source parameters.

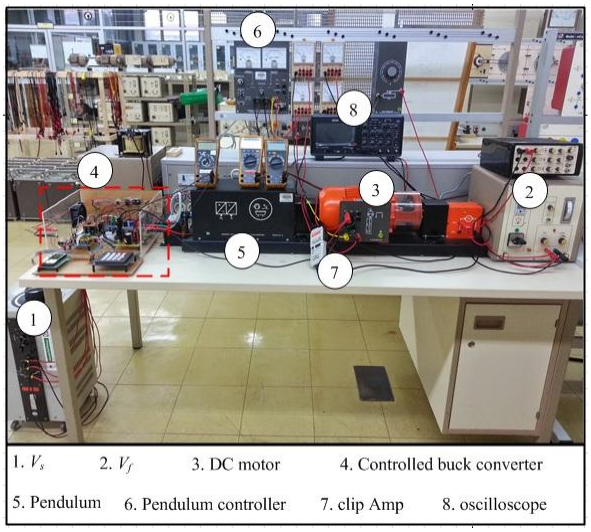

Fig. 4. The experimental test rig

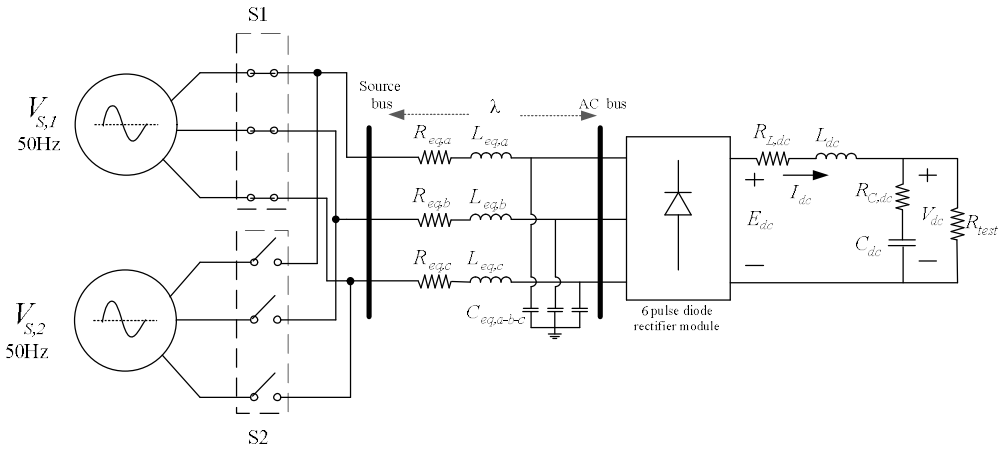

Fig. 5. The testing system for the identification of source parameters

The second part is called the motor parameters. The details how to identify the parameters of both parts are explained as follow:

3.1 Source parameter identifications

The system for the source parameter identification is shown in Fig. 5. In this case, the resistance R_{test} equal to 80 Ω is replaced instead of the controlled speed DC motor as well as in the rig. The resistance and inductance of the DC-link filter ($R_{L,dc}$ and L_{dc}) can be easily measured from the LCR meter. For the rig in Fig. 4, the $R_{L,dc}$ and L_{dc} are equal to 2.1754 Ω and 39.05 mH, respectively. The three-phase line capacitances are very small. They can be set to 2nF for the mathematical model. This is because the DQ mathematical model for the diode rectifier requires a voltage source which can be provided by these capacitances. For the DC-link capacitance, two capacitors 470 µF in series were used. The variation of the capacitance value for each capacitor is from -10% to 50%, typical of electrolytic capacitors. Therefore, to achieve usable parameter values of capacitance ($R_{c,dc}$ and C_{dc}) including line parameters R_{eq} and L_{eq}, a step response test as shown in Fig. 5 was carried out. Switch S_1 and S_2 were used to provide the transient response of V_{dc} when the source voltage is changed from V_{s1} = 80 V_{rms} to V_{s2} = 84 V_{rms}. The transient output voltage responses from the dynamic model of Fig. 5 and from the testing rig of Fig.4 will be called $V_{dc(model)}$ and $V_{dc(experiment)}$, respectively. These responses will be later used in the system identification using the ATS method.

The details of ATS algorithm can be found in [19]-[20]. In this paper, the ATS method is applied to determine the source parameters in which the procedure of the system identification using ATS method is the same as those of the work in [22]. The ATS searching process was conducted 5 trials with random initial solutions. The suitable trial numbers depend on the user. As for this paper, the 5 trials are sufficient to achieve the accurate system parameters. The source parameters from the ATS searching method are given in Table 1 in which the trial 4 can provide the minimum W value.

To validate the results in Table 1, the system in Fig.5 was simulated with the system parameters as given in the trial 4 of the Table 1 including $R_{L,dc}$ = 2.1754 Ω and L_{dc} = 39.05 mH from measurement.

The comparison results between the output voltage responses from the DQ dynamic model and experiment are shown in Fig. 6.

It can be seen in Fig. 6 that a good agreement of the voltage responses between the model and the experiment is achieved. It means that the accurate source parameters can be obtained.

Table 1. The source parameters identified from the ATS algorithm

trials	R_{eq} (µΩ)	L_{eq} (nH)	$R_c$dc (Ω)	C_{dc} (µF)	W
1	96.78	507.02	0.4557	220.03	1.1657
2	98.89	502.23	0.4640	222.22	1.1662
3	99.06	505.21	0.4778	220.77	1.1656
4	94.21	499.99	0.5105	220.11	1.1548
5	93.41	512.10	0.5605	219.17	1.1642

3.2 DC motor parameter identifications

The system for the DC motor parameter identification is shown in Fig. 7 in which V_{dc}, V_f and T_L are equal to 50V, 200V and 0.35 N.m, respectively. The resistance and inductance of the armature and field circuits (R_a, L_a, R_f, and L_f) can be easily measured from the LCR meter. For the rig in Fig.4, the R_a, L_a, R_f, and L_f are equal to 2.78 Ω, 215.5 mH, 591.7 Ω and 136.4 H, respectively. The remain parameters K, B, and J are very complicated to be determined from the measurement. Therefore, these motor parameters will be also identified by ATS algorithm using the same procedure in Section 3(A). Switch S_1 is used to provide the transient responses. From the previous publication [23], this work used only the steady-state speed response for the identification. Hence, the resulting parameters are not accurate. In this paper, the transient speed responses are used in the identification process. Moreover, armature current responses are also included in

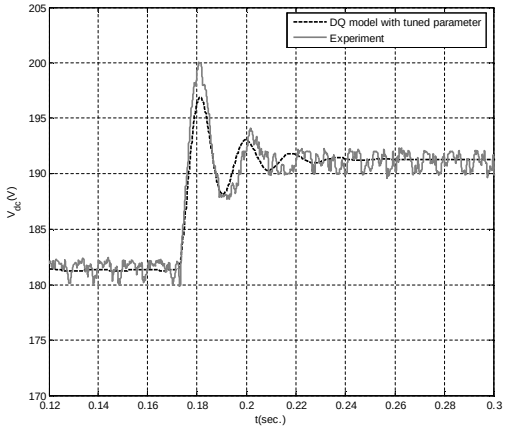

Fig. 6. The comparison results to validate the identified source parameters from the ATS method

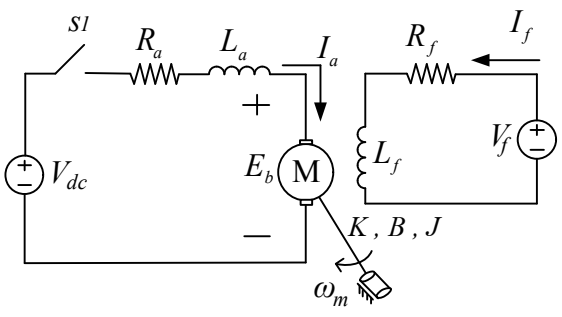

Fig. 7. The testing system for the motor parameter identification

Table 2. The DC motor parameters identified from the ATS algorithm

trials	*K*	*B*	*J*	*W*
1	4.1123	0.002650	0.0112	1.0025
2	4.0785	0.002893	0.0109	1.0011
3	4.2542	0.002712	0.0099	1.0901
4	4.0014	0.002751	0.0120	1.0099
5	4.0536	0.002494	0.0105	1.0121

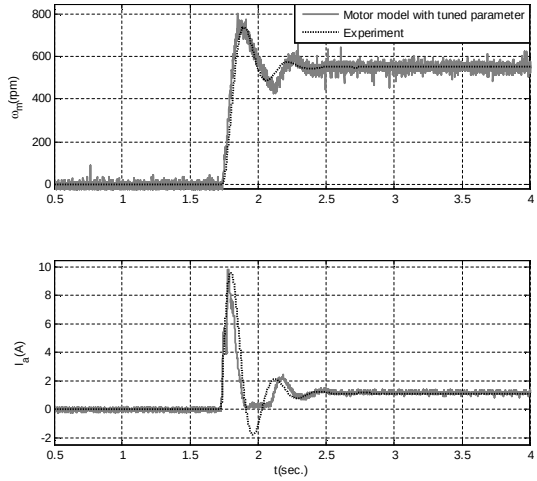

Fig. 8. The comparison results to validate the identified motor parameters from the ATS method

the searching process to improve the accuracy.

The motor parameters from the ATS searching method are given in Table 2. The best DC motor parameter is from the trial 4 in which these values can provide the minimum *W* value.

To validate the results in Table 2, the system in Fig. 7 was simulated with the best motor parameters as given in the trial 4 of the Table 2 including remain parameters from measurement. The comparison results between the output speed and armature current responses from the model and experiment are shown in Fig.8. Note that the model of DC motor is not given in the paper because it is very simple.

It can be seen in Fig. 8 that a good agreement of the transient responses between the DC motor model with parameters from the ATS and the experiment is achieved. It means that the accurate motor parameters can be obtained.

Hitherto, the accurate parameters of considered power system (both source and motor parameters) can be achieved from the ATS method. Therefore, we can use these parameters to validate the linearized model as given in (3) from Section 2 in which this model will be used for the stability analysis in Section 4. All parameters that are used for this validation are as follow: V_s=30 V_{rms}, R_{eq} = 94.21 μΩ, L_{eq} = 499.99 nH, C_{eq} = 2 nF, $R_{L,dc}$ = 2.1754 Ω, $R_{c,dc}$ = 0.5105 Ω, L_{dc} = 39.053 mH, C_{dc} = 220.11 μF, L_b = 15 mH, C_b = 180 μF, R_a = 2.7828 Ω, L_a = 215.5 mH, R_f = 591.7139 Ω, L_f = 136.4 H, K=K_t = K_v = 4.0014, J = 0.0120 kg.m^2 , B = 0.002751, K_p = 5.0768, K_i = 13.4854. Fig.9

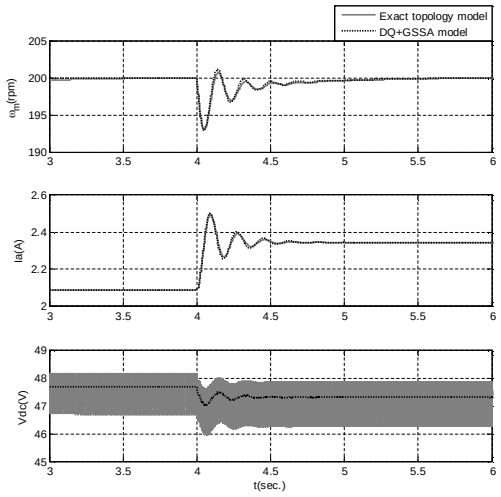

Fig. 9. The model validation for changing load torque

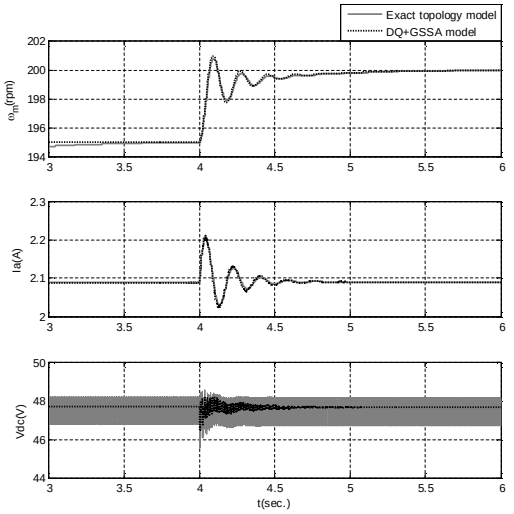

Fig. 10. The model validation for changing speed command

shows ω_m, I_a and V_{dc} waveforms calculated from the linearized model as given in (3) compared with those from the exact topology model to a step change of load torque from 2 N.m. to 2.25 N.m. that occurs at t = 4 s.. Similarly, Fig. 10 shows the same responses when speed command is changed immediately from 195 rpm to 200 rpm at t = 4 s.

From the comparison results in Fig. 9 and Fig. 10, an excellent agreement between the proposed linearized model and the exact topology model is achieved. It confirms that the dynamic model of the system in Fig. 1 derived by the DQ and GSSA methods provides high accuracies in both transient and steady-state responses. In the next section, this resulting model will be used for stability analysis to predict the unstable operation.

4. Stability Analysis

In this section, the linearized model in (3) is then used

with the eigenvalue theorem to analyze the stability. The eigenvalue can be calculated from the Jacobian matrix $\mathbf{A}(\mathbf{x_0}, \mathbf{u_0})$ in (3) by:

$$\det[\alpha \mathbf{I} - \mathbf{A}] = 0 \tag{5}$$

and the system is stable if

$$\mathrm{Re}\{\alpha_i\} < 0 \tag{6}$$

where i =1,2,3,…., n (n = the number of state variables).

To investigate the instability condition due to the CPLs, the eigenvalues of the system with the identified parameters from Section 3 are calculated from the Jacobian matrix when the load torque varies from 0 N.m. to 1.35 N.m. with fixed the speed control natural frequency equal to 22 rad/s and DC motor speed equal to 200 rpm. These eigenvalues are shown in Fig. 11 with the interesting area. According to the eigenvalue theorem, it can be seen in Fig. 11 that the system becomes unstable when the load torque exceeds 0.45 N.m.. To verify the stability result, the intensive time-domain simulation for this case is given in Fig. 12. From the theory, the load torque should not exceed 0.45 N.m. to avoid the unstable operation. Fig. 12 shows that the system becomes unstable when the load torque is equal to 0.9 N.m. (exceed 0.45 N.m.). Referring to Fig. 11 and 12, the unstable eigenvalues are located at ~80 rad/s when the load torque equal to 0.9 N.m. is applied. Therefore, the oscillation having frequency ~80 rad/s (13 Hz) is occurred for the unstable operation. Moreover, the experimental result from the testing rig in Fig. 4 is addressed in Fig. 13 in which the system becomes unstable at load torque equal to 0.9 N.m. (exceed 0.45 N.m.). It can be seen that a good agreement between theoretical, simulation, and experimental results is achieved. Hence, the resulting model with the identified parameters can be used to predict the unstable point with good accuracy. The derived model also allows for convenient analysis of stability margins due to system parameter variations. Normally, engineers can design the desirable value of DC-link inductor and capacitor including the speed control natural frequency. Hence, the effect of these values on the stability margin should be investigated in which these details are addressed in the following sections.

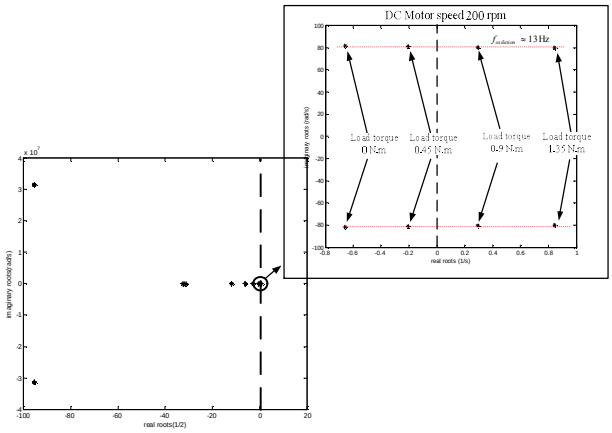

Fig. 11. Eigenvalue plot of load torque variation (ω_n = 22 rad/s)

4.1 Effect of DC-link parameters

Fig. 14 and Fig. 15 shows the effect of changing the dc-link filter parameters for diode rectifier unit on stability in the form of the instability border line. Larger values of inductor and smaller capacitor degrade the stability, i.e., the load torque level at which instability occurs decreased.

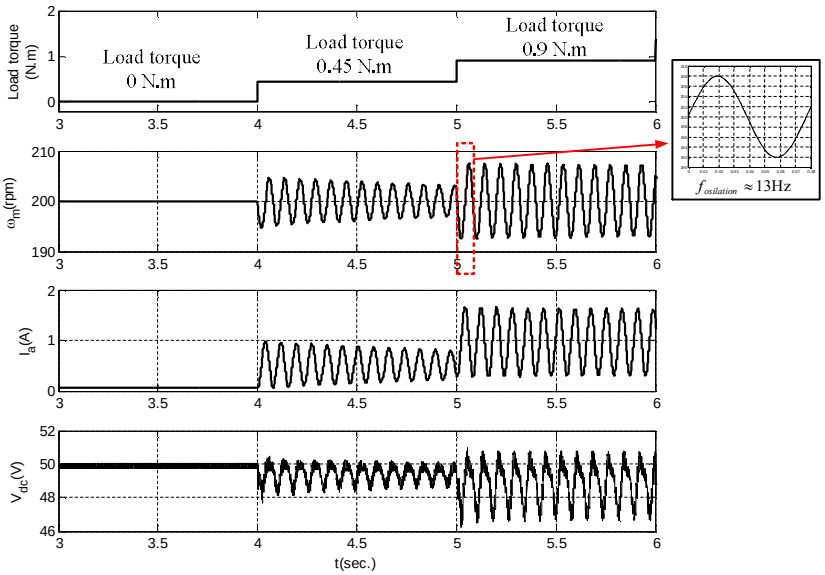

Fig. 12. Simulation results of unstable operation

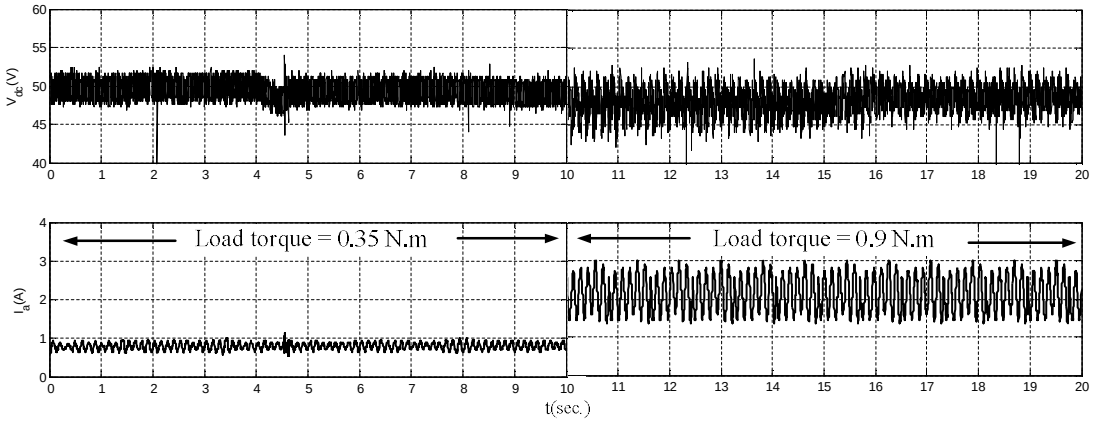

Fig. 13. Experimental results of unstable operation

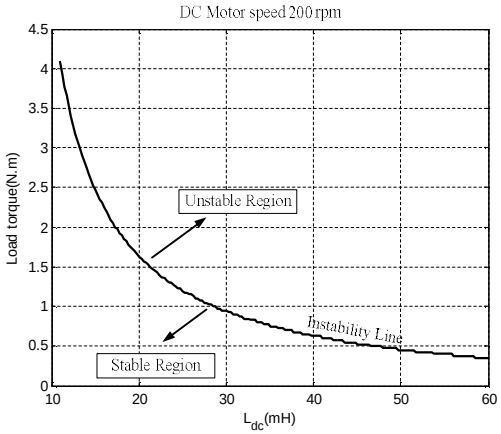

Fig. 14. Instability border for different values of DC-link inductor

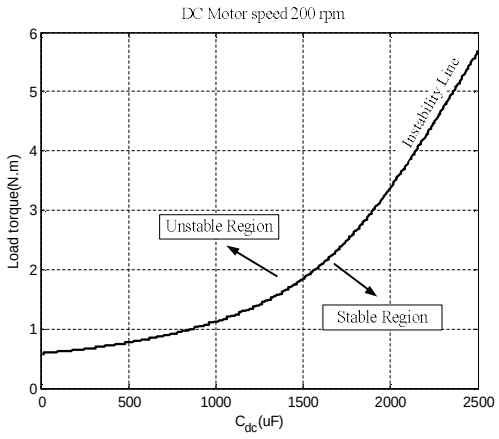

Fig. 15. Instability border for different values of DC-link capacitor

However, there is a matter of certain compromise between the ripple of the signals, weight, cost, and stability. For example, a larger inductor value degrades the stability but provides a smooth dc current, and a larger value of capacitor can improve the stability, however may raise the weight, reliability, and cost issues.

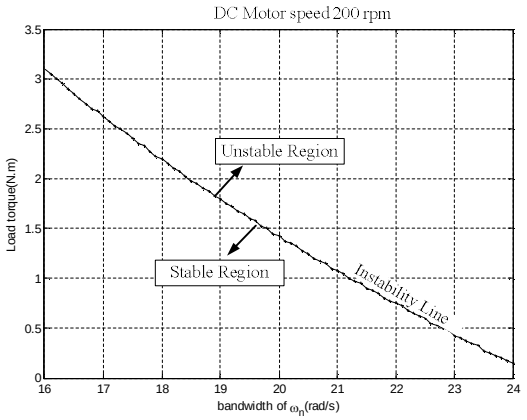

Fig. 16. Instability border for different values of speed control natural frequency

4.2 Effect of speed control natural frequency

In this section the model of (3) is used to assess the effect of speed control natural frequency used in the DC motor drive system. Fig. 16 shows the stability thresholds as the bandwidth of speed loop control is varied. It is clearly seen that decreasing the natural frequency of speed loop control results in significant improve of the stability margin. This is an interesting result since this would appear to be a cheap and effective way of recovering the stability margin.

5. Conclusion

This paper presents how to derive the dynamic model of the three-phase diode rectifier feeding a speed controlled DC motor. The DQ and GSSA methods are used to eliminate the switching behaviour of the power converter in which the DQ method is used to analyze the three-phase rectifier and the GSSA method is also applied to the buck converter. The dynamics of speed loop control are taken into account in the model in which it can be allowed to study the effect of speed control natural ferquency on stability. Moreover, the system identification using the

ATS searching method is also explained to determine the accurate parameters of the practical system. The results show that the proposed dynamic model can correctly predict the unstable point. A good agreement between theoretical prediction, simulation results via the full switching model, and the experimental results is achieved. In addition, the resulting model also allows for convenient analysis of stability margin due to the system parameter variations. The results from this study are very useful for engineers. They can select the appropriate parameters to avoid the unstable point with a good system performance. The concept from this paper can be used to analyze other practical power systems having CPLs such as the AC-DC power system feeding a three-phase induction motor drive circuit. The AC drives with their speed control also behave as a CPL. Therefore, it is very interesting to investigate the effect of bandwidth of speed loop control on the stability margin.

Appendix

The details of Jacobian matrix $\mathbf{A}(\mathbf{x_0},\mathbf{u_0})$, $\mathbf{B}(\mathbf{x_0},\mathbf{u_0})$, $\mathbf{C}(\mathbf{x_0},\mathbf{u_0})$ and $\mathbf{D}(\mathbf{x_0},\mathbf{u_0})$ are as follow:

$$a(5,7)=\frac{K_pR_{C,dc}\omega^*_{m,o}-K_pR_{C,dc}\omega_{m,o}+K_iR_{C,dc}X_{\omega,0}}{A_r\cdot L_{dc}}$$

$$a(6,7)=\frac{-K_p\omega^*_{m,o}+K_p\omega_{m,o}-K_iX_{\omega,0}}{A_r\cdot C_{dc}}$$

$$a(7,6)=\frac{K_p\omega^*_{m,o}-K_p\omega_{m,o}+K_iX_{\omega,0}}{A_r\cdot L_b}$$

$$\mathbf{B}(\mathbf{x_0},\mathbf{u_0})=\begin{bmatrix}
\sqrt{\frac{3}{2}}\frac{\cos\lambda}{L_{eq}} & 0 & 0 & 0\\
\sqrt{\frac{3}{2}}\frac{\sin\lambda}{L_{eq}} & 0 & 0 & 0\\
0 & 0 & 0 & 0\\
0 & 0 & 0 & 0\\
0 & 0 & 0 & \frac{K_pR_{C,dc}I_{L,b0}}{A_rL_{dc}}\\
0 & 0 & 0 & -\frac{K_pI_{L,b0}}{A_rC_{dc}}\\
0 & 0 & 0 & \frac{K_iV_{dc,0}}{A_rL_b}\\
0 & 0 & 0 & 0\\
0 & 0 & 0 & 0\\
0 & \frac{1}{L_f} & 0 & 0\\
0 & 0 & -\frac{1}{J} & 0\\
0 & 0 & 0 & 1
\end{bmatrix}_{12\times4}$$

$$\mathrm{A}(\mathrm{x}_0,\mathrm{u}_0)=\begin{bmatrix}
-\frac{R_{eq}}{L_{eq}} & \omega & -\frac{1}{L_{eq}} & 0 & 0 & 0 & 0 & 0 & 0 & 0 & 0 & 0\\
-\omega & -\frac{R_{eq}}{L_{eq}} & 0 & -\frac{1}{L_{eq}} & 0 & 0 & 0 & 0 & 0 & 0 & 0 & 0\\
\frac{1}{C_{eq}} & 0 & 0 & \omega & -\frac{S_d}{C_{eq}} & 0 & 0 & 0 & 0 & 0 & 0 & 0\\
0 & \frac{1}{C_{eq}} & -\omega & 0 & -\frac{S_q}{C_{eq}} & 0 & 0 & 0 & 0 & 0 & 0 & 0\\
0 & 0 & \frac{S_d}{L_{dc}} & \frac{S_q}{L_{dc}} & -\frac{(r_\mu+R_{L,dc}+R_{C,dc})}{L_{dc}} & -\frac{1}{L_{dc}} & a(5,7) & 0 & 0 & 0 & -\frac{K_pR_{C,dc}I_{L,b0}}{A_r\cdot L_{dc}} & \frac{K_iR_{C,dc}I_{L,b0}}{A_r\cdot L_{dc}}\\
0 & 0 & 0 & 0 & \frac{1}{C_{dc}} & 0 & a(6,7) & 0 & 0 & 0 & \frac{K_pI_{L,b0}}{A_r\cdot C_{dc}} & -\frac{K_iI_{L,b0}}{A_r\cdot C_{dc}}\\
0 & 0 & 0 & 0 & 0 & a(7,6) & 0 & -\frac{1}{L_b} & 0 & 0 & -\frac{K_pV_{dc,0}}{A_r\cdot L_b} & \frac{K_iV_{dc,0}}{A_r\cdot L_b}\\
0 & 0 & 0 & 0 & 0 & 0 & \frac{1}{C_b} & 0 & -\frac{1}{C_b} & 0 & 0 & 0\\
0 & 0 & 0 & 0 & 0 & 0 & 0 & \frac{1}{L_a} & -\frac{R_a}{L_a} & 0 & -\frac{K_vI_f}{L_a} & 0\\
0 & 0 & 0 & 0 & 0 & 0 & 0 & 0 & 0 & -\frac{R_f}{L_f} & 0 & 0\\
0 & 0 & 0 & 0 & 0 & 0 & 0 & 0 & \frac{K_tI_f}{J} & 0 & -\frac{B}{J} & 0\\
0 & 0 & 0 & 0 & 0 & 0 & 0 & 0 & 0 & 0 & -1 & 0
\end{bmatrix}_{12\times12}$$

$$C(x_0,u_0)=\begin{bmatrix}0&0&0&0&1&0&0&0&0&0&0&0\\0&0&0&0&0&1&0&0&0&0&0&0\\0&0&0&0&0&0&0&1&0&0&0&0\\0&0&0&0&0&0&0&0&1&0&0&0\\0&0&0&0&0&0&0&0&0&0&1&0\end{bmatrix}_{5\times12}$$

$$\mathbf{D}(\mathbf{x_0},\mathbf{u_0})=\begin{bmatrix}0&0&0&0\\0&0&0&0\\0&0&0&0\\0&0&0&0\\0&0&0&0\end{bmatrix}_{5\times4}$$

Nomenclature

AC	Alternating current
ATS	Adaptive Tabu search
CCM	Continuous conduction mode
CPL	Constant power load
DC	Direct current
GSSA	Generalized state-space averaging method
AI	Artificial intelligent
V_s	Source voltage
$R_{eq,abc}$	Resistance of transmission line
$L_{eq,abc}$	Inductance of transmission line
$C_{eq,abc}$	Capacitance of transmission line
$I_{in,abc}$	Input current of diode bridge rectifier
λ	Phase shift angle between source bus and AC bus
α	Eigenvalue of matrix $\mathbf{A}(\mathbf{x_0},\mathbf{u_0})$
$E_{dc,1}$	Output voltage of diode bridge rectifier
$R_{L,dc}$	Inner resistance of L filter
r_μ	Virtual resistance in diode bridge rectifier
L_{dc}	Inductance of L filter at DC bus
I_{dc}	Output current of diode bridge rectifier
$R_{C,dc}$	Inner resistance of C filter
C_{dc}	Capacitance of C filter at DC bus
V_{dc}	DC bus voltage
ω_m	Speed of DC motor
T_L	Load torque in DC motor
L_b	Inductance of buck converter
C_b	Capacitance of buck converter
	V_a Armature voltage in DC motor
R_a	Armature resistance in DC motor
L_a	Armature inductance in DC motor
I_a	Armature current in DC motor
E_b	Back electromotive force (Back EMF) in DC motor
R_f	field resistance in DC motor
L_f	field inductance in DC motor
I_f	field current in DC motor
V_f	field voltage in DC motor
V_{sd}	Source voltage on d axis
V_{sq}	Source voltage on q axis
I_{sd}	Source current on d axis
I_{sq}	Source current on q axis
$V_{bus,d}$	Bus voltage on d axis
$V_{bus,q}$	Bus voltage on q axis
d	duty cycle
K_p	Proportional gain
K_i	Integral gain
K_t , K_v	Constant value of DC motor
B	Viscosity coefficient of DC motor
J	Moment of inertia in DC motor
A_r	Amplitude of carrier signal

Acknowledgements

This work was supported by Suranaree University of Technology (SUT).

References

[1] J. Santana, J.L. Naredo, F. Sandoval, I Grout and O.J. Argueta, "Simulation and Construction of Speed Control for a DC Motor. Mechatronics," *World Applied Sciences Journal*, vol. 12, pp. 1145-1156, 2002.

[2] C. Rivetta, G.A. Williamson and A. Emadi, "Constant Power Loads and Negative Impedance Instability in Sea and Undersea Vehicles," *Statement of the Problem and Comprehensive Large-Signal Solution IEEE Electric Ship Tech. Symposium.*, 2005, pp. 313-320.

[3] R.D. Middlebrook, "Input Filter Consideration in Design and Application of Switching Regulator," *in Proc. IEEE Industry Application Society Annual Meeting*, Chicago, Illinois, October 1976, pp. 366-382.

[4] A. Emadi, A. Khaligh, C.H. Rivetta and G.A. Williamson, "Constant Power Loads and Negative Impedance Instability in Automotive Systems," *Modeling Stability and Control of Power Electronic Converters and Motor Drives IEEE Trans. on Vehicular Tech.,* pp. 1112-1125, 2006.

[5] A. Emadi, "Modeling of Power Electronic Loads in AC Distribution Systems Using the Genearlized State-Space Averaging Method," *IEEE Trans. on Indus. Elect.,* vol. 51, no. 5, pp. 992-1000, October 2004.

[6] L. Han, J. Wang, and D. Howe, "State-space average modelling of 6- and 12-pulse diode rectifiers," in *Proc. The 12th European Conf. on Power Elect. and Appl.,* Aalborg, Denmark, pp. 1-10. Sep. 2007.

[7] J. Flower and C. Hodge, "Stability and transient-behavioural assessment of power-electronics-based dc-distribution systems Part I: The root-locus technique," *Journal of Marine Engineering and Technology.,* no. A5, pp. 13-21.

[8] L. Ying-xi, M. Xin-hua, G. Hong-juan, and J. Hua,

"Stability study and simulation analysis on aircraft transformer rectifier unit (TRU) with constant power load (CPL)," *ICEMS 2005*, Sept. 2005, vol. 3, pp. 2018-2022.

[9] K-N. Areerak, S.V. Bozhko, G.M. Asher and D.W.P. Thomas, "Stability analysis and modelling of AC-DC system with mixed load using DQ-transformation method," *IEEE International Symposium on Industrial Electronics*, 2008, pp. 19-24.

[10] K-N. Areerak, S.V. Bozhko, G.M. Asher and D.W.P. Thomas, "DQ-transformation approach for modelling and stability analysis of AC-DC power system with controlled PWM rectifier and constant power loads," *Power Electronics and Motion Control Conference*, 2008, pp. 2049-2054.

[11] C.T. Rim, N.S. Choi, G.C. Cho and G.H. Cho, "Complete DC and AC Analysis of Three Phase Controlled-Current PWM Rectifier Using Circuit D-Q Transformation," *IEEE Trans. on Power Electronics*, pp. 390-396, 1994.

[12] P. Ngamkong, P. Kochcha, K-N Areerak, S. Sujitjorn and K-L. Areerak, "Application of the generalized state-space averaging method to modeling of DC-DC Power Converters," *Mathematical and Computer Modelling of Dynamical Systems*, vol. 18, no. 3, pp. 243-260, June 2012.

[13] J. Mahdavi, A. Emadi, M.D. Bellar and M. Ehsani, "Analysis of power electronic converters using the generalized state space averaging approach," *IEEE Transactions on Circuits and Systems I: Fundamental Theory and Applications*, vol. 44, no. 8, pp. 767-770, Aug. 1997.

[14] A. Emadi, "Modeling of Power Electronic Loads in AC Distribution Systems Using the Genearlized State-Space Averaging Method," *IEEE Trans. on Indus. Elect.*, vol. 51, no. 5, pp. 992-1000, October 2004.

[15] J. Flower and C. Hodge, "Stability and transient-behavioural assessment of power-electronics-based dc-distribution systems Part I: The root-locus technique," Journal of Marine Engineering and Technology., no. A5 2004, pp. 13-21.

[16] L. Han, J. Wang and D. Howe, "Stability Assessment of Distributed DC Power Systems for 'More Electric' Aircraft," in Proc. Power Electronics, Machines and Drives (PEMD 2008), York St John University College, York, UK, 2-4 April 2008, pp. 661-665.

[17] S.D. Sudhoff, S.F. Glover, P.T. Lamm, D.H. Schmucker and D.E. Dellisle, "Admittance Space Stability Analtsis of Power Electronic Systems," IEEE Trans. on Aerospce and Electronic Systems, vol. 36, no. 3, pp. 965-972, July 2000.

[18] J. Pakdeeto, K.-N. Areerak, and K.-L. Areerak, "The Optimal Controller Design of Buck-Boost Converter by using Adaptive Tabu Search Algorithm Based on State-Space Averaging Model," *Journal of Electrical Engineering & Technology,* vol. 12, no. 3, pp. 1146-1155, 2017.

[19] T. Kulworawanichpong, K-L. Areerak, K-N. Areerak, P. Pao-la-or, D. Puangdownreong, and S. Sujitjorn, "Dynamic parameter identification of induction motors using intelligent search techniques," *IASTED International Conference on Modelling, Identification, and Control (MIC2005)*, Innsbruck, Austria: February 16-18, 2005, pp. 328-3320.

[20] D. Puangdownreong, K.-N. Areerak , A. Srikaew and S. Sujitjorn, "System identification via Adaptive Tabu Search," Industrial Technology, *IEEE ICIT '02*, International Conference on 11-14 Dec. 2002, Vol.2, pp. 915-920.

[21] T. Sopapirm, K-N. Areerak, K-L. Areerak, "Stability Analysis of AC Distribution System with Six-Pulse Diode Rectifier and Multi-Converter Power Electronic Loads," *International Review of Electrical Engineering* (*I.R.E.E.*), vol. 6, no. 7 (Part A), November-December 2011, pp. 2919-2928.

[22] T. Sopapirm, K-N. Areerak and K-L. Areerak, "The Identification of AC-DC Power System Parameters Using an Adaptive Tabu Search Technique," *International Review of Electrical Engineering (I.R.E.E.)*, July-August 2012, vol. 7, no. 4, pp. 4655-4662.

[23] S. Udomsuk, K-L. Areerak, K-N. Areerak, A. SriKaew, "Parameters identification of separately excited DC motor using adaptive tabu search technique," *Advance in Energy Engineering(ICAEE) 2010)*, Beijing, China: June 19-20, 2010, pp.48-51.

Jakkrit Pakdeeto was born in Nakhon Ratchasima, Thailand, in 1991. He received the B.Eng. (first-class honors) and M.Eng. degrees in electrical engineering from Suranaree University of Technology (SUT), Nakhon Ratchasima, Thailand, in 2013 and 2015, respectively where he is currently studying the Ph.D. degree in electrical engineering. His main research interests include stability analysis, power electronics, AI applications, control systems and DC micro-grid systems.

Kongpan Areerak received the B.Eng. M.Eng degrees from Suranaree University of Technology (SUT), Nakhon Ratchasima, Thailand, in 2000 and 2001, respectively and the Ph.D. degree from the University of Nottingham, Nottingham, UK., in 2009, all in electrical engineering. In 2002, he was a lecturer in the Electrical and Electronic Department,

Rangsit University, Thailand. Since 2003, he has been a Lecturer in the School of Electrical Engineering, SUT. He received the Associate Professor in Electrical Engineering in 2015. His main research interests include system identifications, artificial intelligence applications, stability analysis of power systems with constant power loads, modeling and control of power electronic based systems, and control theory.

Kongpol Areerak received the B.Eng, M.Eng, and Ph.D. degrees in electrical engineering from Suranaree University of Technology (SUT), Thailand, in 2000, 2003, and 2007, respectively. Since 2007, he has been a lecturer and Head of Power Quality Research Unit (PQRU) in the School of Electrical Engineering, SUT. He received the Associate Professor in Electrical Engineering in 2015. His main research interests include active power filter, harmonic elimination, artificial intelligence applications, motor drive, and intelligence control systems.